

Variable Bandwidth Image Denoising Using Image-based Noise Models

Noura Azzabou^{1,2} Nikos Paragios¹ Frédéric Guichard² Frédéric Cao²

(1) MAS, Ecole Centrale de Paris, Grande Voie des Vignes, 92295 Chatenay-Malabry, France

(2) DxOLabs, 3 Rue Nationale, 92100 Boulogne, France

noura.azzabou@ecp.fr, nikos.paragios@ecp.fr, fguichard@dxo.com, fcaco@dxo.com

Abstract

This paper introduces a variational formulation for image denoising based on a quadratic function over kernels of variable bandwidth. These kernels are scale adaptive and reflect spatial and photometric similarities between pixels. The bandwidth of the kernels is observation-dependent towards improving the accuracy of the reconstruction process and is constrained to be locally smooth. We analyze the evolution of the noise model from the RAW space to the RGB one, by propagating it over the image formation process. The experimental results demonstrate that the use of a variable bandwidth approach and an image intensity dependent noise variance ensures better restoration quality.

1. Introduction

Denoising is still an open problem in image processing. Its great challenge is dealing with rich content like texture. Traditional techniques rely on a simple noise model like the additive white Gaussian noise with constant variance (AWGN), and often assume constant scale. Both assumptions are quite unrealistic and often violated in practice, in particular when observing natural images with various content.

State of the art techniques in image enhancement refer to local methods, image decomposition in orthogonal spaces, partial differential equations as well as complex mathematical models. Filters and morphological operators are the most prominent local approaches [17, 25, 27, 2, 3] and exploit homogeneity of the image through convolution. Global methods represent images through a set of invertible transformations of an orthogonal basis [20, 7, 16] or a specific designed dictionary [8]. Then noise is removed through the modification of the coefficients with limited importance in the reconstruction process.

Partial differential equations methods incorporate more structure in the denoising process where the noise-free images correspond to the steady state solution of the PDE. Global approaches based on the minimization of objective

functions and in particular the total variation [22, 24, 14] are efficient tools in the image enhancement field. Nevertheless, these approaches are based on a local smoothness hypothesis and fail to preserve texture. In order to address this problem, separating structure from texture is the most prominent technique to deal with such limitation and has gained significant attention in the past years [1, 26, 21]. In spite of their performance, these methods fail to separate noise from texture. In fact, like noise, texture is an oscillatory pattern. Furthermore, these models are complex and rely on a data fidelity term that cannot be computed directly and can be only approximated.

In this paper, we propose a variational formulation where the regularization term is based on the weighted laplacian of the image. The underlying image model introduces linear relations between pixels with interactions that are governed by weights reflecting photometric similarities and geometric distances. The level of interaction is spatially varying through a variable bandwidth spatial kernel that adapts the regularization neighborhood to the texture scale. Parallel to that, we demonstrate that the noise model is different from the AWGN and its explicit recovery requires knowledge of the entire image conversion chain. To overcome this limitation, we learn the variation of noise through calibration patterns formed with homogeneous square patches and use this model towards more realistic denoising.

The paper is organized as the following: the second section is devoted to the introduction of denoising model. Next, we discuss the propagation of a linear noise model through the image conversion chain leading to a more realistic noise assumption. In section 4, we address the problem of image denoising in the RGB space. Discussion and conclusions are part of the last section.

2. Variational Image Denoising

Total variation minimization has been a dominant formulation for image denoising. One can find in the literature several variants of the original model with respect to the data fidelity and the regularization components. Variational formulation of the NLmean and the bilateral filter [15] was

recently introduced, but the minimized functional are not convex. In [9], a tractable quadratic formulation was proposed that is based on the assumption that the underlying image model is piecewise constant for similar pixels. Scale selection has not been considered in these methods. In this section we will introduce a new regularization functional that addresses this limitation.

2.1. Model Introduction

Let us assume that the neighborhood of a pixel \mathbf{x} is the entire image domain Ω . This implies that all pixels of the image domain can be used to reconstruct the original signal at a given pixel. The reconstruction is performed through the minimization of an energy function composed of a regularization term and a fidelity to data constraint. The regularization term is defined as:

$$E_{reg}(I) = \int_{\Omega} \left(\left[\frac{1}{Z(\mathbf{x})} \int_{\Omega} w(\mathbf{x}, \mathbf{y}) I(\mathbf{y}) d\mathbf{y} \right] - I(\mathbf{x}) \right)^2 d\mathbf{x} \quad (1)$$

Where, $w(\mathbf{x}, \mathbf{y})$ are symmetric weights that reflect the similarity between neighboring pixels and $Z(\mathbf{x}) = \int_{\Omega} w(\mathbf{x}, \mathbf{y}) d\mathbf{y}$ is a normalization factor. The regularization term that we consider in the present model corresponds to the integration over the image domain of the squared weighted laplacian in each pixel. This model suggests that a pixel can be approximated by a linear combination of other image pixels and we think that such model is more accurate than a piecewise constant one. A similar regularization form was recently considered in [6] without any local constraints in the context of image deblurring.

The definition of similarity refers to photometric resemblance and spatial vicinity between pixels. The weight expression considered in our paper is

$$w(\mathbf{x}, \mathbf{y}) = \exp \left(-\frac{d(f(\mathbf{x}), f(\mathbf{y}))^2}{2\sigma_{ph}^2} \right) \exp \left(-\frac{\|\mathbf{x} - \mathbf{y}\|^2}{2\sigma_s^2} \right) \quad (2)$$

The first term $d(f(\mathbf{x}), f(\mathbf{y}))$, where f is the noisy observed image, reflects the photometric distance between the content observed in these pixels. One possible expression for this term is the L_2 distance between patches centered at \mathbf{x} and \mathbf{y} . The choice of this distance is motivated by its robustness to noise. The second term represents the geometric Euclidean distance between them in the image domain. The parameters σ_{ph} and σ_s are variables that determine the bandwidth of the photometric kernel and the spatial one. We will focus in the following section on the importance of the selection of the spatial bandwidth.

As far as the fidelity constraint is concerned it insures that the restored image is close to the observed one. The introduction of a constraint on the residual image is a popular tool [19, 10] to satisfy such a demand.

$$\int_{\Omega} (f(\mathbf{x}) - I(\mathbf{x}))^2 d\mathbf{x} = \sigma_n^2 \quad (3)$$

where σ_n is the noise standard deviation, f is the observed image and I is the restored one. Such a constraint has to be satisfied during the reconstruction process. It can be expressed in the form of a distance between reconstruction and observation leading to the following objective function

$$E(I) = \lambda \int_{\Omega} (f(\mathbf{x}) - I(\mathbf{x}))^2 d\mathbf{x} + \int_{\Omega} \left(\left[\frac{1}{Z(\mathbf{x})} \int_{\Omega} w(\mathbf{x}, \mathbf{y}) I(\mathbf{y}) d\mathbf{y} \right] - I(\mathbf{x}) \right)^2 d\mathbf{x} \quad (4)$$

with λ being a coefficient that determines the importance of the fidelity to data component in the energy.

The energy function is quadratic, thus convex and reaches a unique minimum. Starting from the initial condition $I_0 = f$, we perform a gradient descent as follows

$$I^{t+1} = I^t - dt \nabla E \quad (5)$$

where the derivative of the objective function with respect to the image is;

$$\nabla E = 2 \int_{\Omega} \left(\int_{\Omega} \frac{w(\mathbf{z}, \mathbf{y})}{Z(\mathbf{z})} I(\mathbf{y}) d\mathbf{y} - I(\mathbf{z}) \right) \frac{w(\mathbf{z}, \mathbf{x})}{Z(\mathbf{z})} d\mathbf{z} + 2 \left(I(\mathbf{x}) - \int_{\Omega} \frac{w(\mathbf{x}, \mathbf{y})}{Z(\mathbf{x})} I(\mathbf{y}) d\mathbf{y} \right) + 2\lambda(I(\mathbf{x}) - f(\mathbf{x})) \quad (6)$$

In order to enforce the constraint obtained from the assumption on the noise model, an iterative process is used that alternates between the two conditions. Starting from a fixed value $\lambda = \lambda_0$, and when the energy reaches its minimum we have:

$$2\lambda(I - f) + \nabla E_{reg} = 0 \quad (7)$$

where ∇E_{reg} refers to the first two terms in the energy gradient expression (6). Then we can write

$$2\lambda(I - f)^T(I - f) + (I - f)^T \nabla E_{reg} = 0. \quad (8)$$

Knowing that $(I - f)^T(I - f) = \sigma_n^2$, λ can be updated according to:

$$\lambda = \frac{(f - I)^T \nabla E_{reg}}{2\sigma_n^2} \quad (9)$$

Once λ is updated, we restart the minimization process with the new value of λ until convergence.

2.2. Bandwidth Selection

Our model involves weights that reflect the similarity between pixels and the interaction between them during the process of image denoising. The selection of the spatial bandwidth is crucial in the regularization process. In [12], it has been proven that the choice of the convolution kernel bandwidth is important for the accuracy of the intensity estimation in the case of the NLmean algorithm [5]. The increase of the kernel size reduces the variance of the estimator while increasing its bias. The spatial kernel bandwidth

needs to be adapted to each pixel in the image in order to obtain an optimal balance between precision and good match to the actual pixel intensity. Therefore, minimizing the cost function (4) with respect to a pixel dependent spatial bandwidth $\sigma_s(\mathbf{x})$ results in a more adapted selection. Under the assumption that image content at the very local scale is coherent, one can also consider that the spatial bandwidth is also regular and smooth. Therefore, the use of a smoothness term (the L_2 norm of the gradient of $\sigma_s(\mathbf{x})$) during the estimation of the bandwidth $\sigma_s(\mathbf{x})$ is a natural choice. Thus we aim to minimize the following objective function:

$$E(I, \sigma_s) = \lambda \int_{\Omega} (f(\mathbf{x}) - I(\mathbf{x}))^2 d\mathbf{x} + \mu \int_{\Omega} \|\nabla \sigma_s(\mathbf{x})\|^2 d\mathbf{x} + \int_{\Omega} \left(\left[\frac{1}{Z(\mathbf{x})} \int_{\Omega} w(\mathbf{x}, \mathbf{y}, \sigma_s(\mathbf{x})) I(\mathbf{y}) d\mathbf{y} \right] - I(\mathbf{x}) \right)^2 d\mathbf{x} \quad (10)$$

The minimum of this cost function is computed using the steepest gradient descent according to

$$\sigma_s^{t+1} = \sigma_s^t - dt \frac{\partial E}{\partial \sigma_s(\mathbf{x})} \quad (11)$$

with the derivatives of the objective function being given by

$$\frac{\partial E}{\partial \sigma_s(\mathbf{x})} = 2\mu \Delta \sigma_s + 2 \left(\frac{1}{Z(\mathbf{x})} \int_{\Omega} w(\mathbf{x}, \mathbf{y}) I(\mathbf{y}) d\mathbf{y} - I(\mathbf{x}) \right) \mathcal{G}(\mathbf{x}) \quad (12)$$

with $\mathcal{G}(\mathbf{x})$ being,

$$\begin{aligned} &= \frac{\partial}{\partial \sigma_s(\mathbf{x})} \left[\frac{1}{Z(\mathbf{x})} \int_{\Omega} w(\mathbf{x}, \mathbf{y}, \sigma_s) I(\mathbf{y}) d\mathbf{y} - I(\mathbf{x}) \right] \\ &= \frac{[\int_{\Omega} \|\mathbf{x} - \mathbf{y}\|^2 w(\mathbf{x}, \mathbf{y}) I(\mathbf{y}) d\mathbf{y}] [\int_{\Omega} w(\mathbf{x}, \mathbf{y}, \sigma_s) d\mathbf{y}]}{\sigma_s^3 [\int_{\Omega} w(\mathbf{x}, \mathbf{y}, \sigma_s) d\mathbf{y}]^2} \\ &\quad - \frac{[\int_{\Omega} w(\mathbf{x}, \mathbf{y}) I(\mathbf{y}) d\mathbf{y}] [\int_{\Omega} \|\mathbf{x} - \mathbf{y}\|^2 w(\mathbf{x}, \mathbf{y}, \sigma_s) d\mathbf{y}]}{\sigma_s^3 [\int_{\Omega} w(\mathbf{x}, \mathbf{y}, \sigma_s) d\mathbf{y}]^2} \end{aligned} \quad (13)$$

Image denoising and bandwidth selection are addressed in an iterative fashion through alternating the spatial bandwidth update and minimization of the cost function (4). An example of bandwidth selection is shown in [Fig.(1)] where a certain qualitative interpretation regarding the behavior of the process can be extracted. Scale selection in edges and texture regions corresponds to lower values than smooth homogeneous regions, which is a natural outcome.

2.3. Experimental Validation

One can now use the theoretical framework introduced in the previous section for image enhancement. This method is based on a total variation minimization with a regularization function based on variable bandwidth kernel. Toward objective validation of our method, we have used natural images corrupted by a synthetic Gaussian noise $\sigma_n =$



Figure 1. (a) Original image (b) the bandwidth value associated to it

{10, 20}. We compared our approach to well known filtering techniques such as unsupervised based patch regularization [12], the bilateral filter [25], the Non Local Mean approach [5], the total variation (TV) [24] and the anisotropic diffusion (AD) [23] using an edge stopping function of the type $(1 + |\nabla I|^2 / K^2)^{-1}$. The parameters of the considered methods were adjusted to get a good balance between texture preserving and noise suppression as well as the highest possible Peak Signal to Noise Ratio (PSNR) values. As far as our method is concerned, we restricted the neighborhood size to a 15×15 window instead of the whole image domain to decrease computation time. The initial value of λ is 0.02. The photometric bandwidth σ_{ph} is fixed according to the noise level ($\sigma_{ph}=15$ for $\sigma_n=20$ and $\sigma_{ph}=8$ for $\sigma_n=10$).

Regarding quantitative validation, we used the PSNR criterion defined by

$$PSNR = 10 \log_{10} \frac{255^2}{MSE} \quad MSE = \frac{1}{|\Omega|} \sum_{\mathbf{x} \in \Omega} (I_0(x) - I(x))^2$$

where I_0 is the noise-free ideal image and I its estimation by the denoising process.

In table [1], we present experimental validation results for the different methods on a set of images corrupted by additive Gaussian noise. PSNR values show that our restoration method as well as the one proposed in [12] outperforms all the other ones. These two methods are based on a variable spatial bandwidth. Therefore, one can conclude that a better estimation of intensity is closely related to the better selection of bandwidth.

Concerning subjective evaluation criteria, we consider the whole aspect of the image in terms of noise suppression and small details preservation. Visual comparison results of denoising [Fig.(2), (3)] show that in spite of the high value of PSNR, the method proposed in [12] fails to preserve small details. One can see in the residual image [Fig.(3)] that our residual component is close to the Gaussian noise and free of image details contrarily to the other method. In [Fig.(4)] we can see another result of restoration where the variable bandwidth NLmean method results in an oversmoothed image while we keep some amount of noise in our denoised image. Thus, the selection of one of these two methods is dependent on the use of the resulting images.

Despite the promising results obtained from our ap-

	Barbara	Boat	Fingerprint	House	Lena	Baboon	Peppers
our Method	30.46	29.94	27.65	32.34	32.12	26.02	30.67
KB06 [12]	30.37	30.12	28.16	32.90	32.64	26.29	30.59
NLmean	28.78	28.92	26.45	30.86	31.13	25.18	29.05
TV	26.18	27.72	26.08	28.43	28.45	25.18	28.51
AD	26.45	28.06	24.81	29.41	29.27	23.68	-
Bilateral	26.75	27.82	24.12	29.18	29.28	24.95	28.88

Table 1. PSNR values for denoised images (The PSNR of the image corrupted by Gaussian noise of std=20 is equal to 22.15)

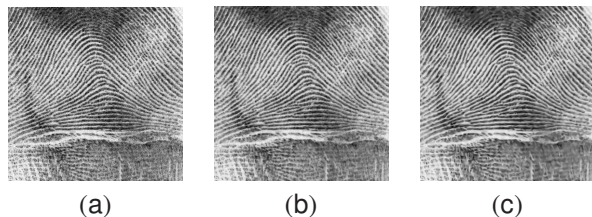


Figure 2. (a) Noisy image corrupted by white noise (b) restored image using KB06 [12] (c) restored one using our method

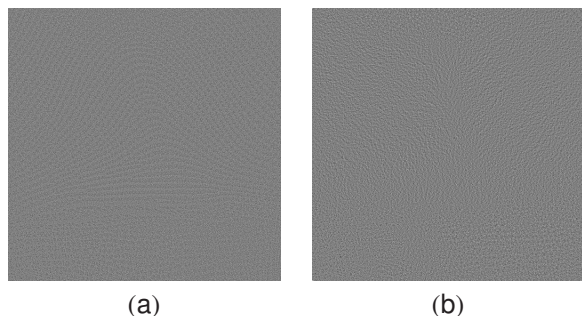


Figure 3. The difference between the noisy image and the restored one (a) using KB06 [12] (b) using our Method

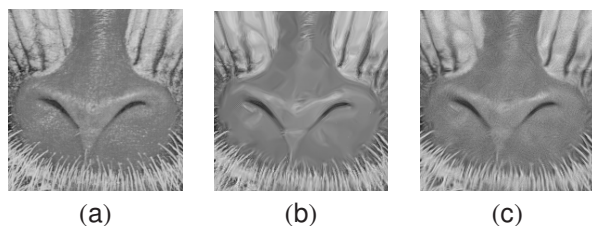


Figure 4. (a) Original image (b) restored image using KB06 [12] (c) restored one using our method

proach, one has to address a major limitation that is the noise model selection. Gaussian additive noise models with fixed variance are often considered in the literature for the RGB space. In the next section, we aim to study the noise model evolution during the conversion from the RAW image, composed of Bayer pattern, to the final RGB one.

3. Noise Properties in RGB Image

Our approach is motivated by the fact that in the RAW space one can see a dependency between the noise model and the observation. In the image denoising literature, most

of the approaches rely on the assumption of an additive white noise with fixed standard deviation. Our aim is to demonstrate that such an assumption is far from being realistic and also to consider a noise model that is adequate for natural images.

The RAW image is the one obtained from the impact of light photons on the camera sensor. This image is corrupted by noise due to three perturbation sources [28], the photon noise, the dark noise and the spatial noise. The photon noise refers to the fluctuation of the number of photons that reach the pixel. The Noise variance is a linear function of the photons number and thus linear with the pixel intensity. The dark noise is generated by the leakage current and independent of the pixel intensity. The spatial noise is related to the fact that pixels are not perfectly similar and behave in a different way. This component has a quadratic dependency on the pixel intensity. Under all these considerations, the noise model can be approximated with a Gaussian noise with variance

$$\sigma_n^2(I) = \alpha I^2 + \beta I + \gamma \quad (14)$$

The conversion of the RAW values to the RGB space is obtained through a processing chain. Such a procedure consists of three major steps; (i) white balance correction, (ii) interpolation/demosaicing, (iii) color adjustment and Gamma correction.

Noise Propagation & White Balance

Such a process consists in multiplying each pixel in the Bayer pattern by a constant coefficient to homogenize intensity in gray regions. The output image noted wI is defined as

$$wI_R = \alpha_r I_R, \quad wI_G = \alpha_g I_G, \quad wI_B = \alpha_b I_B \quad (15)$$

It is important to note that before white balance, the variance does only depend on pixel intensity and not on pixel color. In other words, a green pixel, a red or a blue one will have the same noise variance as long as their intensity is the same. After white balance this is no longer the case and we have the following relation.

$$\sigma_n(wI_c)^2 = \alpha_c^2 \sigma_n(I_c)^2 \quad \text{where } c \in \{R, G, B\} \quad (16)$$

Noise Propagation & Demosaicing

The demosaicing step consists in recovering the missing color information for each pixel [13, 4]. If we consider the example of a green pixel, one has to find the corresponding red and blue intensities. A very basic way is to perform a linear interpolation using neighboring pixels.

$$\begin{aligned} dI_R(x, y) &= \frac{wI_R(x-1, y) + wI_R(x+1, y)}{2} \\ dI_B(x, y) &= \frac{wI_B(x, y-1) + wI_B(x, y+1)}{2} \end{aligned} \quad (17)$$

where dI is the new obtained image after interpolation. In this particular case and if we suppose that $wI_R(x-1, y) \approx wI_R(x+1, y)$ we have

$$\sigma_n^2(dI_R(x, y)) \approx \frac{\sigma_n^2(wI_R(x-1, y))}{2} \quad (18)$$

One can notice from expression (18) that the variance of an interpolated pixel is the half of the variance of a pixel whose intensity was measured by the sensor. This example shows that the noise variance depends on the pixel's intensity, color and position.

Noise Propagation & Color

The color transformation is applied to the image in order to obtain a color rendering close to the photographed scene. This transformation is linear and has the following form

$$\begin{aligned} MC \cdot dI &= cI, \\ dI &= (dI_R, dI_G, dI_B)^T, \quad cI = (cI_R, cI_G, cI_B)^T \end{aligned} \quad (19)$$

where MC is 3×3 color matrix transformation and dI is the intensity vector after demosaicing. The covariance matrix associated to the noise after this transformation is

$$\sigma_n^2(cI) = MC \cdot \Sigma_n^2(dI) \cdot MC^T \quad (20)$$

Where $\Sigma_n^2(dI)$ is the diagonal matrix with $\sigma_n^2(dI_R)$, $\sigma_n^2(dI_G)$, $\sigma_n^2(dI_B)$ being its coefficients.

This expression suggests that color transformation introduces interchannel correlation between noise components. The final processing step is the Gamma correction to map the histogram of the image and enhance the contrast mainly in dark regions. This transformation is a non linear operation which makes noise modeling more complex.

Through our description of a very basic image conversion chain, we were able to demonstrate that the noise model differs significantly from the commonly used white Gaussian noise with a fixed variance. So, there is a strong interest in performing the process on the RAW space where explicit, reasonable and realistic models can be considered. Nevertheless, in some situations one does not have access to these information and has only the RGB image with no knowledge of the transformation process.

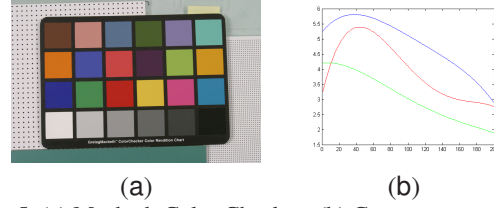


Figure 5. (a) Macbeth Color Checkers (b) Curve corresponding to the evolution of standard deviation of the noise with respect to the intensity for each channel Red, Green and Blue

4. Denoising RGB Images

Noise model estimation from images has been an open problem for the past two decades. Two techniques are mostly present in the literature, the use of theoretical models (like white noise) which is dominant and the inference of the model from the images [18, 11]. For example in [18], the authors introduce a method to estimate the noise model and its variation with pixel intensity. This model relies on a learning step using many camera response functions. We propose an alternative approach that assumes a rather weak calibration stage of the camera. The process consists in shooting a calibration pattern (Macbeth Color Checkers), an image that consists of rectangular homogeneous regions with various colors and intensities. Then, for each calibration patch we associate a noise variance. This variance can be approximated by the image variance inside the patch. The calibration image [Fig.(5)] is composed of 24 patches corresponding to 24 different intensities for each channel. An interpolation is performed to derive the missing noise variance relative to all possible intensity values in the range $[0..255]$. We can see the obtained empirical curve that represents the variation of noise variance for each channel for the Canon 10D digital camera in [Fig.(5)]. It is important to point out that our noise estimation method requires only knowledge about shooting conditions which makes it more flexible with respect to the camera model.

Such empirical and non-parametric noise models can now be used to provide a constraint in the image reconstruction process.

$$\begin{aligned} E_{reg}(I, \sigma_s) &= \mu \int_{\Omega} \|\nabla \sigma_s(\mathbf{x})\|^2 d\mathbf{x} \\ &+ \int_{\Omega} \left(\left[\frac{1}{Z(\mathbf{x})} \int_{\Omega} w(\mathbf{x}, \mathbf{y}, \sigma_s(\mathbf{x})) I(\mathbf{y}) d\mathbf{y} \right] - I(\mathbf{x}) \right)^2 d\mathbf{x} \end{aligned} \quad (21)$$

subject to the constraint

$$\int_{\Gamma(GL_i)} (f(\mathbf{x}) - GL_i)^2 d\mathbf{x} = \sigma_n^2(GL_i)$$

Where GL_i is the gray level that ranges between $\{0..255\}$ and $\Gamma(GL_i)$ is the level line of the image I associated to the intensity GL_i . The update of the parameters λ_i is then

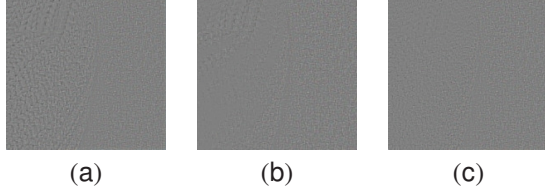


Figure 7. Difference between the noisy image and the restored one using (a) our method with fixed noise variance $\sigma_n^2 = 4$ (b) Image restored using the NLmean algorithm (c) Image restored using our method with variable noise variance

performed according to

$$\lambda_i = \frac{\int_{\mathbf{x} \in \Gamma(GL_i)} (f(\mathbf{x}) - GL_i) \nabla E_{reg}(\mathbf{x}) dx}{2\sigma_n^2(GL_i)} \quad (22)$$

One can notice here that the fidelity to data term is different for each intensity. Furthermore, it is inversely proportional to the noise standard deviation, which means that each level line in the image is processed in a different manner according to the corresponding noise intensity.

4.1. Validation

In order to evaluate the performance of our method, we have considered several examples of noisy image patches relative to different cameras. We compared the quality of the restoration provided by the NLmean algorithm and our algorithm in case of variable noise variance and fixed noise variance. The parameters of each method were set to suppress the maximum amount of noise while preserving details and texture. For RGB images, we must point out that each channel is denoised separately using the same parameters for the three channels. Nevertheless, in the case of variable noise variance, we considered a different noise curve for each channel. In figure [Fig.(6), (7)], we can see that for the denoising approaches based on a fixed noise parameter the white texture is oversmoothed and this is shown by the details present in the residual image. Our proposed method relies on a variable data term coefficient, where we use a high fidelity term in the white region and a small one in the dark regions. This behavior is implied by equation (22) where the value of λ_i is inversely proportional to the noise standard deviation. The same conclusion holds for the example shown in figure [Fig.(8),(9)] with a different Camera (Nikon D70). We notice that with variable noise variance the texture is preserved in the light colored regions. This confirms that a better denoising must take into account the evolution of noise with image intensity.

5. Discussion

In this paper we have proposed a novel technique for image denoising. Our main contribution consists of defining a

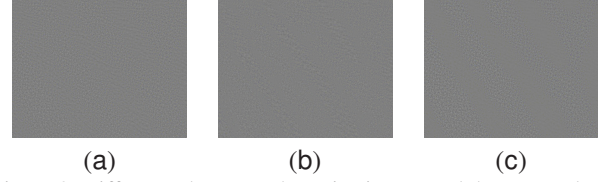


Figure 9. Difference between the noisy image and the restored one using (a) our method with fixed noise variance $\sigma_n^2 = 5$ (b) Image restored using the NLmean algorithm (c) Image restored using our method with variable noise variance

more realistic image model, an automatic bandwidth selection process and more realistic noise assumptions. We have demonstrated the potentials of the method on synthetic and real noise. Our method has outperformed most of the existing state of the art methods.

Better bandwidth selection is a critical step in our approach. The process incurs a bias due to the initial condition for the bandwidth selection. Therefore, we aim to introduce some notions of classification between texture and flat regions. Such classification could be either used to improve the initial conditions on the bandwidth selection or introduce a more appropriate objective function component that takes into account this classification. As far as it concerns the image model, we have considered linear interpolation. The use of non-linear models would increase complexity but in some sense could improve the model performance in particular when modeling complex structures like microtexture. A future step will be the use of image adapted dictionaries towards better definition of the photometric distance between pixels.

References

- [1] J. Aujol, G. Gilboa, T. Chan, and S. Osher. Structure-texture image decomposition - modeling, algorithms, and parameter selection. *International Journal of Computer Vision*, 67(1):111–136, 2006.
- [2] N. Azzabou, N. Paragios, and F. Guichard. Random walks, constrained multiple hypotheses testing and image enhancement. In *ECCV*, pages 379–390, 2006.
- [3] N. Azzabou, N. Paragios, and F. Guichard. Uniform and textured regions separation in natural images towards mpm adaptive denoising. In *SSVM*, 2007.
- [4] E. Bennett, M. Uyttendaele, C. Zitnick2, R. Szeliski, and S. Kang. Video and image bayesian demosaicing with a two color image prior. In *ECCV*, pages 508–521, 2006.
- [5] A. Buades, B. Coll, and J.-M. Morel. A non-local algorithm for image denoising. In *CVPR*, pages 60–65, 2005.
- [6] A. Buades, B. Coll, and J.-M. Morel. Image enhancement by non-local reverse heat equation. Technical report, CMLA Preprint N 2006-22, 2006.
- [7] M. Do and M. Vetterli. Pyramidal directional filter banks and curvelets. In *ICIP01*, pages III: 158–161, 2001.
- [8] M. Elad and M. Aharon. Image denoising via learned dictionaries and sparse representation. In *CVPR*, pages 895–900, 2006.

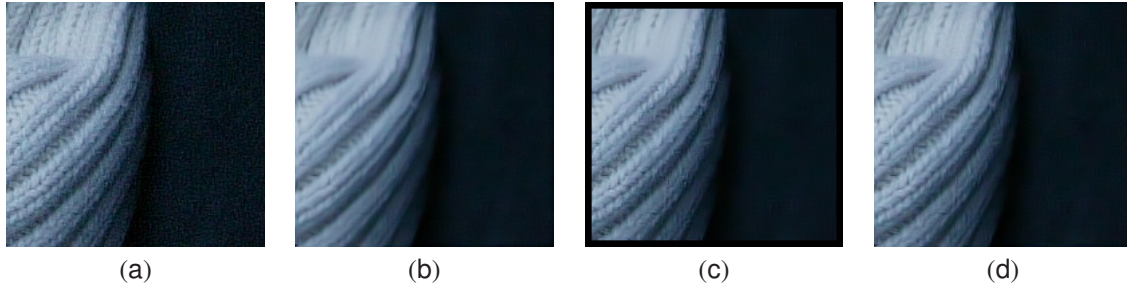


Figure 6. (a) Original noisy image (b) Image restored using our method with fixed noise variance $\sigma_n^2 = 4$ (c) Image restored using the NLmean algorithm (d) Image restored using our method with variable noise variance

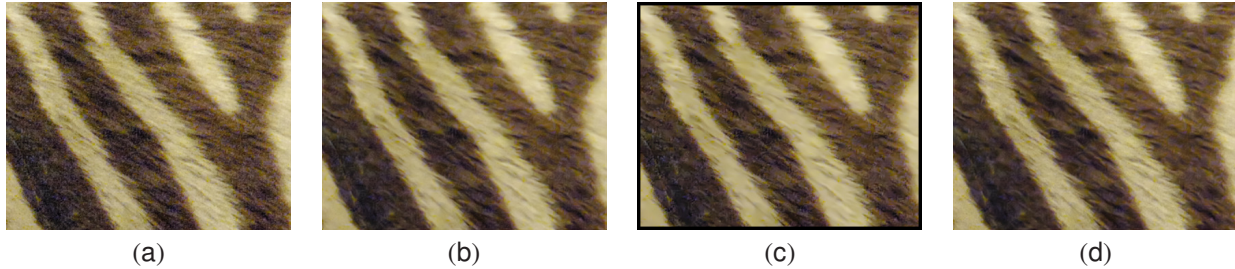


Figure 8. (a) Original noisy image (b) Image restored using our method with fixed noise variance $\sigma_n^2 = 5$ (c) Image restored using the NLmean algorithm (d) Image restored using our method with variable noise variance

- [9] G. Gilboa and S. Osher. Nonlocal linear image regularization and supervised segmentation. Technical report, UCLA CAM Report 06-47, 2006.
- [10] G. Gilboa, N. Sochen, and Z. Y.Y. Variational denoising of partly-textured images by spatially varying constraints. *IEEE Transactions on Image Processing*, 24(8):2281–2289, 2006.
- [11] G. Healey and R. Kondepudy. Radiometric ccd camera calibration and noise estimation. *IEEE Transaction on Pattern Analysis and Machine Intelligence*, 16(3):267–276, 1994.
- [12] C. Kervrann and J. Boulanger. Unsupervised patch-based image regularization and representation. In *ECCV*, pages 555–567, 2006.
- [13] R. Kimmel. Demosaicing: Image reconstruction from color CCD samples. *IEEE Transaction on Image Processing*, 8(9):1221–1228, 1999.
- [14] R. Kimmel, R. Malladi, and N. Sochen. Image processing via the beltrami operator. In *ACCV*, pages 574–581, 1998.
- [15] S. Kindermann, S. Osher, and P. Jones. Deblurring and denoising of images by nonlocal functionals. *SIAM Multiscale Modeling and Simulation*, 4:1091–1115, 2005.
- [16] E. Le Pennec and S. Mallat. Sparse geometric image representations with bandelets. *IEEE Transactions on Image Processing*, pages 423–438, 2005.
- [17] S. Lee. Digital image smoothing and the sigma filter. *CVGIP*, 24(2):255–269, November 1983.
- [18] C. Liu, W. Freeman, R. Szeliski, and S. Kang. Noise estimation from a single image. In *CVPR*, pages 901–908, 2006.
- [19] F. Malgouyres. Minimizing the total variation under a general convex constraint for image restoration. *IEEE Transaction on Image Processing*, 11(12):1450–1456, 2002.
- [20] S. Mallat. A theory for multiscale signal decomposition: The wavelet representation. *IEEE Transactions on Pattern and Machine Intelligence*, pages 674–693, 1989.
- [21] Y. Meyer. *Oscillating Patterns in Image Processing and Non-linear Evolution Equations: The Fifteenth Dean Jacqueline B. Lewis Memorial Lectures*. American Mathematical Society, Boston, MA, USA, 2001.
- [22] D. Mumford and J. Shah. Optimal Approximation by Piecewise Smooth Functions and Associated Variational Problems. *Communications on Pure and Applied Mathematics*, 42:577–685, 1989.
- [23] P. Perona and J. Malik. Scale space and edge detection using anisotropic diffusion. *IEEE Transactions on Pattern and Machine Intelligence*, 12:629–639, 1990.
- [24] L. Rudin, S. Osher, and E. Fatemi. Nonlinear Total Variation Based Noise Removal. *Physica D*, 60:259–268, 1992.
- [25] C. Tomasi and R. Manduchi. Bilateral filtering for gray and color images. In *ICCV*, pages 839–846, 1998.
- [26] L. Vese and S. Osher. Modeling Textures with Total Variation Minimization and Oscillating Patterns in Image Processing. *Journal of Scientific Computing*, 19:553–572, 2003.
- [27] L. Vincent. Morphological grayscale reconstruction in image analysis: Applications and efficient algorithms. *IEEE Transactions on Image Processing*, 2:176–201, 1993.
- [28] C.-C. Wang. *A Study of CMOS Technologies for Image Sensor application*. PhD thesis, MIT, 2001.